RSC Advances

PAPER

View Article Online
View Journal | View Issue

Cite this: *RSC Adv.*, 2017, **7**, 46229

Preparation and characterization of an ultrafine HMX/NQ co-crystal by vacuum freeze drying method

Han Gao,[a] Qinghua Wang,*[b] Xiang Ke,[a] Jie Liu,[a] Gazi Hao,[a] Lei Xiao,[a] Teng Chen,[a] Wei Jiang *[a] and Qiao'e Liu[c]

Received 14th June 2017
Accepted 18th September 2017

DOI: 10.1039/c7ra06646e

rsc.li/rsc-advances

In this paper a new energetic co-crystal consisting of 1,3,5,7-tetranitro-1,3,5,7-tetrazacyclooctane (HMX) and nitroguanidine (NQ) was prepared using a vacuum freeze drying method. Scanning electron microscopy (SEM) revealed that the particle size was under 500 nm and the morphology was spherical. Fourier transform infrared spectroscopy (FT-IR) and Raman spectroscopy suggest that hydrogen bonds exist between HMX and NQ molecules. Powder X-ray diffraction spectra (PXRD) indicated the product was different from the single components and their mechanical mixture. Thermal gravimetric analysis and differential scanning calorimetry (TGA/DSC) were employed to characterize the thermal behavior of the co-crystal and then the related thermodynamic parameters were calculated, which indicated that after co-crystallization the molecule of the co-crystal needed more energy to activate. The result of an impact sensitivity test indicated that the sensitivity was effectively reduced compared to neat HMX and the mechanical mixture. The density of the product was found to be 1.80 g cm^{-3} and the storage performance was also investigated.

1. Introduction

Energetic materials (explosives, propellants and pyrotechnics) are widely used by the military and in civil applications, but the existing elemental explosives can't meet the high energy and low sensitivity requirements at the same time. There are three principal means to lower the sensitivity: improving crystal quality,[1–3] ultrafine treatment[4] and polymer coating.[5] But these methods all have their own shortcomings, like complex steps, high costs and energy reduction. Therefore, it is necessary to find a new type of less sensitive explosive with high energy. HMX has a larger density, higher detonation velocity and higher detonation heat than cyclotrimethylenetrinitramine (RDX).[6–9] HMX even has a better chemical stability than that of TNT, which is known as one of the explosives with the best explosion performance. But a high mechanical sensitivity restricts its wide application. NQ, which is called the cold explosive, has slightly better detonation properties than those of TNT (104% TNT equivalence). Due to its low explosion temperature and low sensitivity, NQ based gun propellant are adopted by many countries in modern long-range heavy caliber artillery.[10–12]

A co-crystal is a multicomponent molecular crystal composed of two or more kinds of neutral molecular constituents with fixed stoichiometric ratio bonded by intermolecular hydrogen bonds, π-stacking, and van der Waal's forces or other non-covalent effects.[13–16] Co-crystal technology has been widely used for the pharmaceutical chemicals due to their functions of improving the solubility, bioavailability physical and chemical stability properties of drugs with their chemical structure unchanged.[17–23] Therefore, co-crystal technology is a promising way to be used in the area of energetic materials. In recent ten years, more and more energetic co-crystals were prepared and characterized[24–26] like CL-20/TNT,[27] HMX/TATB,[28] CL-20/DNT,[29] CL-20/BTF,[30] CL-20/HMX[31] and CL-20/TATB.[32] However, most of these co-crystals which were prepared by solvent method are micro-sized particles with uncontrollable morphology. Therefore, these new co-crystals cannot meet the requirements for military and civilian applications. It is urgent to find a new method to prepare ultrafine co-crystals. Vacuum freeze drying has been used in materials preparation[33,34] and been proved effective in the energetic area to drying explosives prepared by liquid phase method.[35] Its principle is to freeze the solvent in the material to solid state and then make the solvent sublimate directly under vacuum condition to achieve the purpose of drying. The fine particles of material can't grow and reunite in solid state solvent so that vacuum freeze drying is an effective way to prepare micro and nano-sized material. Besides, vacuum freeze drying is safer than spray drying and simpler than bead milling presented by Wang[36] and Qiu[37] respectively. Herein, we

[a]School of Chemical Engineering, Nanjing University of Science and Technology, Nanjing 210094, PR China. E-mail: superfine_jw@126.com

[b]No. 763 Military Representive Office, Taiyuan 030000, China. E-mail: wqh001@tom.com

[c]Gansu Yinguang Chemical Industry Group Co., Ltd., Baiyin 730900, China

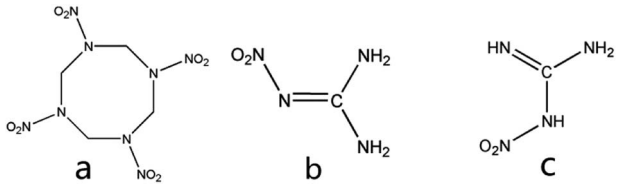

Fig. 1 Molecular structures of (a) HMX and (b, c) two forms of NQ.

prepared ultrafine HMX/NQ co-crystal using vacuum freeze drying method. HMX is an eight membered ring formed with four C and four N atoms and four $-NO_2$ in a HMX molecule which has four crystal forms α, β, γ and δ. The first two are stable at room temperature. HMX also forms solvates with some solvents like NMP, DMI and PNO. The molecular structures of HMX and NQ are shown in Fig. 1. NQ has only one structure (b) but in a solution it can has two different forms (b) and (c).

2. Experimental methods

2.1. Chemicals and materials

β-HMX was produced by Gansu Yinguang Chemical Industry Group Co. Ltd. NQ was provided by Liaoning Qingyang Chemical Industry Corporation Group Co. Ltd of China. Dimethylformamide (DMF), analytical reagent, was produced by Shanghai Lingfeng Chemical Reagent Co. Ltd.

2.2. Sample preparation

0.0296 g HMX and 0.0104 g NQ (molar ratio 1 : 1) were added to 10 mL DMF. After being uniformly mixed and dissolved after 1 hour ultrasonic agitation, the beaker of mixed explosive solution was put into a CHRIST Alpha 2-4 LD plus freeze drying instrument by the cover of filter paper. The main parameters of main drying process were that the temperature was set −45 °C and the vacuum degree was set 0.050 mbar respectively. After two days drying, the solvent completely sublimated and the HMX/NQ white ultrafine co-crystal was obtained.

2.3. Characterization

The scanning electron microscopic (SEM) morphology characterization was performed with a Hitachi S-4800. Fourier transform infrared spectroscopy (FT-IR) was determined by a Thermo Fisher Nicolet iS10 FT-IR Spectrometer with working range from 4000 to 500 cm^{-1}. Micro-Raman spectroscopy (MRS) was carried out on a HORIBA JOBIN YVON S.A.S. LABRAM Aramis with working range from 4000 to 100 cm^{-1}. The excitation source was a 532 nm laser (2.33 eV). X-ray diffraction (XRD) was carried out with a Bruker Instruments D8 Advance system in the 2θ range of 5–70° at a scan rate of 0.02° s^{-1} with Cu-$K_{\alpha 1}$ radiation (λ = 0.15406 nm) operated at 40 kV and 40 mA. A SDT Q600 was employed to do the thermal gravimetric analysis/differential scanning calorimetry (TGA/DSC). 1–2 mg sample was weighed into an alumina crucible each time. Test conditions were a 20 mL min^{-1} nitrogen purge flow at different heating rate from 25 to 400 °C. For comparison, the mechanical mixture of HMX and NQ (molar ratio 1 : 1) was also tested for all the tests. The mechanical mixture of HMX and NQ was prepared by solvent drop grinding. The weighed raw materials were put into a mortar. Then after dropping some ethyl acetate, the materials were grinded together for some minutes. After drying process, the mechanical mixture was obtained.

2.4. Sensitivity test

Impact sensitivity is an important index to measure the mechanical sensitivity properties of explosives. Impact sensitivity of samples was measured and evaluated according to GJB-772A-97 standard method 601.1.[38] Impact sensitivity was measured by the drop hammer apparatus made by De Kong Corporation. The testing conditions of impact sensitivity are as follows: the weight of dropping hammer was 2 kg the height was 25 cm and the quantity of sample was 30 ± 1 mg. Twenty five repeating cycles were tested. As a reference, the physical mixture of HMX and NQ at 1 : 1 molar ratio was also tested.

2.5. Density test

Density is one of the most important factors of explosives for applications. We used drainage method according to GJB-772A-97 standard method 402.2 (ref. 38) to measure and calculate the density of NQ, HMX and the co-crystal. First, measure 2 mL liquid (50% ethanol) in a cylinder (accuracy 0.1 mL) then measure a certain mass simple (accurate to 0.01 g) and add in the cylinder slowly. Finally, after standing for an hour, read the volume change. So the density can be calculated by mass divided by volume.

2.6. Storage test

The storage performance of our product was tested by mercury pressure gauge method according to GJB-772A-97 standard method 501.1.[38] The heating temperature was set 100 °C and the heating time was 45 h. The mercury pressure gauge was used to measure the pressure of released gas under constant volume and certain vacuum conditions. Then the pressure was converted to volume under standard conditions. Before the test, the simples were dried in a 55 °C and 9–12 kPa vacuum oven.

3. Results and discussion

3.1. Morphology characterization

As show in Fig. 2, NQ represents needle crystal or crystalline powder. β-HMX particles are irregular polyhedrons with uneven size and a very wide distribution range. Most of the particles are 50 μm or more in diameter. However, ultrafine HMX/NQ co-crystals are spherical and most of the particle sizes are under 500 nm. Compared with the raw materials, the as-prepared co-crystal has little edges which are advantageous for the reduction of mechanical sensitivity.[39,40]

3.2. FT-IR

The FT-IR spectra of NQ, HMX, the co-crystal and the mixture are shown in Fig. 3. The assignments of the major bonds are

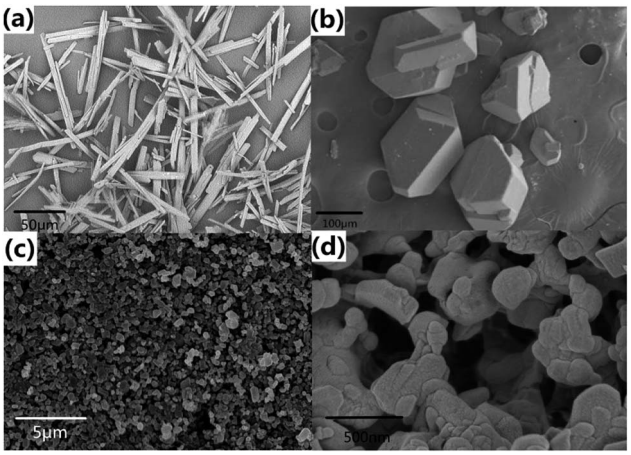

Fig. 2 SEM of (a) NQ; (b) HMX and (c, d) HMX/NQ co-crystal.

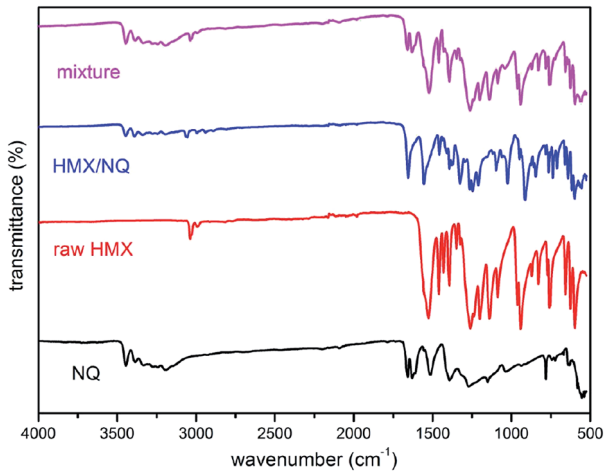

Fig. 3 Infrared absorption spectra of NQ, HMX, ultrafine HMX/NQ co-crystal and the mechanical mixture.

shown in Table 1. First, the main absorption peaks of both NQ and HMX can be observed in the spectra of the co-crystal and the mixture which proves that the as-prepared material and the mixture were consisted of NQ and HMX. Second, some of the main absorption peaks have shifted more or less in the spectra of the co-crystal but hardly shifted in the mixture. The curve of the mixture is more like a superposition of HMX and NQ. For example, NQ has the bands at 3445.21 cm^{-1} and 3384.94 cm^{-1} which are the stretch vibration absorption peaks of $-NH_2$. However, these peaks shifted to 3447.61 cm^{-1} and 3391.21 cm^{-1} respectively in the co-crystal but remain unchanged in the mixture. Similarly, the stretch vibration absorption peaks of –CH– in HMX and the mixture are both at 3036.85 cm^{-1} while it shifted to 3054.21 cm^{-1} in the co-crystal. Besides, assignments of ring bending 942.06 cm^{-1} and stretching 961.82 cm^{-1} in HMX shifted to 935.79 cm^{-1} and 949.29 cm^{-1} respectively in the co-crystal while hardly shifted in the mixture. More peak changes can be seen in the Table 1. The difference between FT-IR absorption peaks of the co-crystal and the mixture can be attributed to the formation of intermolecular hydrogen bonding, which causes the electron density of molecules to change.

3.3. Raman spectroscopy

Raman spectroscopy is a useful tool for characterization of co-crystals. The Raman spectra of NQ, HMX, HMX/NQ co-crystal

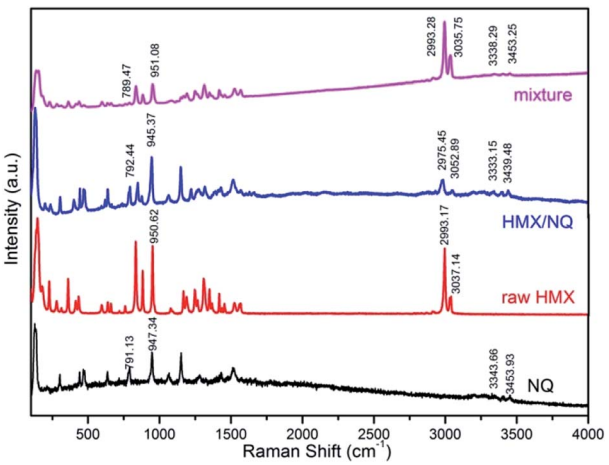

Fig. 4 Raman spectra of NQ, HMX, ultrafine HMX/NQ co-crystal and the mechanical mixture.

Table 1 Assignments (cm^{-1}) of the major bands from 4000 cm^{-1} to 500 cm^{-1} of the infrared absorption spectra of NQ, HMX, HMX/NQ co-crystal product and the mixture

Assignments	NQ	Mixture	Co-crystal	HMX	Assignments
$-NO_2$ out-of-plane bending	781.51	781.51	781.51	771.39	$-NO_2$ out-of-plane bending
		942.54	935.79	942.06	Ring bending
		961.82	949.29	961.82	Ring stretching
		1324.38	1326.30	1324.86	CH_2 bending
$-NO_2$ symmetric stretching	1393.32	1393.32	1393.80	1393.80	$-NO_2$ symmetric stretching
		1459.85	1457.44	1459.37	CH_2 bending
$-NO_2$ asymmetric stretching	1514.33	1523.00	1555.31	1552.90	$-NO_2$ asymmetric stretching
C–N stretching (C=N)	1657.52	1658.48	1655.12		
		3036.85	3054.21	3036.85	C–H stretching
N–H stretching	3385.91	3385.42	3390.24		
N–H stretching	3445.21	3445.21	3447.61		

and the mechanical mixture are presented in Fig. 4. The results indicated that both NQ and HMX are detected in the co-crystal and the mixture. But similar to the results of FT-IR, absorption peaks of both NQ and HMX have different degrees of shift in the curve of the co-crystal but not in the curve of the mixture. As shown in Fig. 4, NQ has bands at 3343.66 cm^{-1} and 3453.93 cm^{-1} which related to the $-NH_2$ stretching. However, the two bands shift to 3333.15 cm^{-1} and 3439.48 cm^{-1} in the co-crystal. HMX has bands at 2993.17 cm^{-1} and 3037.14 cm^{-1} (C–H stretching) which shift to 2975.45 cm^{-1} and 3052.89 cm^{-1} respectively. This can also be observed in the fingerprint area of the spectrum which has marked in Fig. 3. All these changes may be attributed to the hydrogen bond interactions between NQ and HMX molecules in the co-crystal.

3.4. PXRD

The PXRD patterns of NQ, raw HMX, HMX/NQ co-crystal, the mechanical mixture, two polymorphs of HMX and the HMX/DMF solvate are presented in Fig. 5. As show in the figure the as-prepared co-crystal can be distinguished from the single components *via* powder X-ray diffraction. The as-prepared co-crystal has main diffraction angles at 8.6°, 13.0°, 17.2° and 28.2° which are different from the single component and other possible polymorphs and solvates. Moreover, some of the peaks for NQ and HMX have disappeared. For example, the main diffraction angles of NQ located at 17.7°, 30.7°, 37.8° and 45.2° which cannot be observed in the pattern of the co-crystal. Similarly, the main diffraction angles of raw HMX localized at 14.7°, 16.1°, 23.1° and 32.0° also disappeared after co-crystallization. For comparison, the XRD data of mechanical mixture, was tested which was obviously the superposition of the two raw materials. The raw HMX was β crystal form compared with the β-HMX PXRD pattern. The results indicated that the formation of co-crystal changes the symmetry of crystal structure. Every crystal has its own unique powder diffraction pattern, after forming a co-crystal the characteristic peaks of each single component disappear while new diffraction peaks arise. PXRD is a useful means to distinguish polymorphic and solvated forms. So we compared the XRD of the as-prepared co-crystal with that of PDF #00-045-1539 β-HMX, #00-042-01769 α-HMX and the HMX/DMF solvate. The result proved the formation of the HMX/NQ co-crystal.

3.5. TGA/DSC

The TG curves of NQ, HMX, HMX/NQ co-crystal and the mixture are shown in Fig. 6. As shown in the figure, HMX/NQ co-crystal and the mixture both have two weight loss steps which belong to NQ and HMX respectively which is in accordance with the CL-20/TNT co-crystal prepared by Yang.[41] But the co-crystal has a decomposition advance compared with the mixture, which can be attributed to the formation of hydrogen bonding. The result revealed that the co-crystal has a different decomposition behaviour from the two components and the mechanical mixture.

The DSC thermograms of NQ, HMX, and HMX/NQ co-crystal are shown in Fig. 7. As shown in Fig. 7, NQ and HMX both has obvious decomposition peak. However, there are two thermal decomposition peaks (DP1 and DP2) in the DSC curve of the co-crystal which belong to NQ and HMX respectively. However, DP1 and DP2 appear lower temperatures in the co-crystal compared to the single component at the same heating rate. The apparent activation energy of each sample can be calculated according to the Kissinger correlation

$$\ln\left(\frac{\beta}{T_P^2}\right) = \ln\left(\frac{AR}{E_a}\right) - \frac{E_a}{RT_P} \quad (1)$$

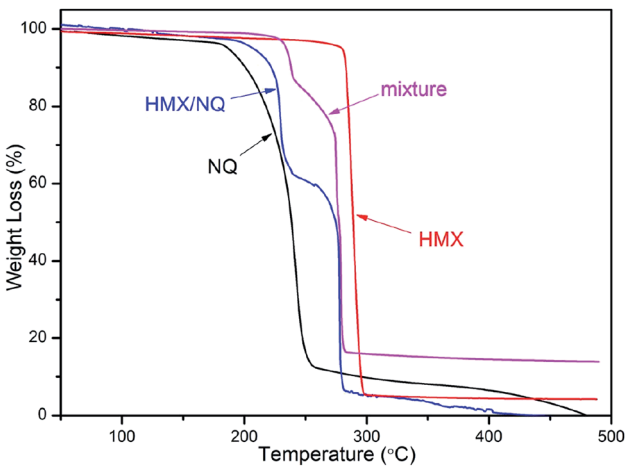

Fig. 6 TG curves of NQ, HMX, HMX/NQ co-crystal and the mixture at 5 °C min^{-1} heating rate.

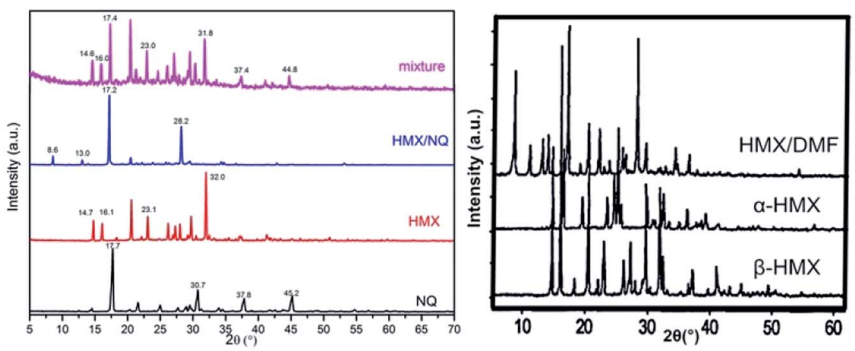

Fig. 5 PXRD patterns of NQ, raw HMX, HMX/NQ co-crystal, the mechanical mixture, two polymorphs of HMX and the HMX/DMF solvate.

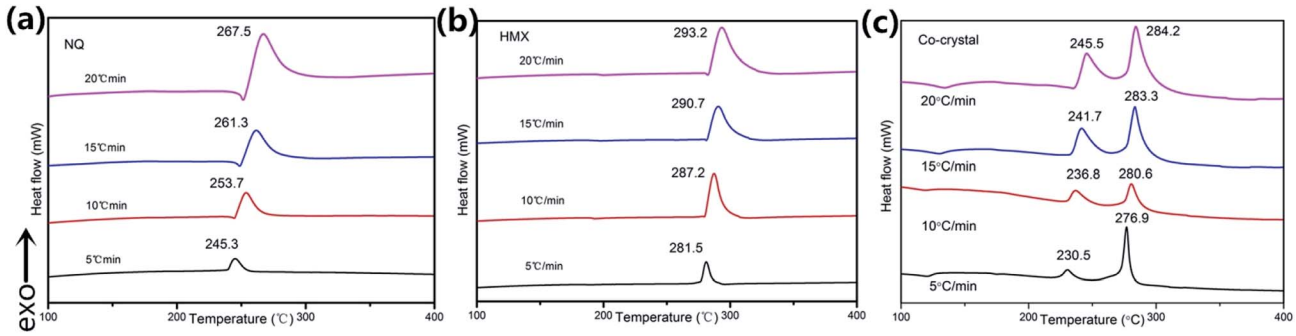

Fig. 7 DSC curves of (a) NQ, (b) HMX and (c) HMX/NQ co-crystal.

where β is the heating rate in degrees Kelvin per minute, T_P is the decomposition peak temperature in degrees Kelvin, E_a is the apparent activation energy, R is the ideal gas constant and A is the pre-exponential factor. According to the eqn (1), the term $\ln(\beta/T_P^2)$ varies linely with $1/T_P$. By drawing the line of function one can use the slope to calculate the apparent activation energy. Fig. 8 shows the function graphs of NQ, HMX and the co-crystal.

The activation enthalpy ($\Delta H^{\neq}$), the activation entropy ($\Delta S^{\neq}$) and the Gibbs free energy ($\Delta G^{\neq}$) can be calculated according to eqn (2)–(4) below.[42]

$$A\exp\left(-\frac{E_k}{RT_P}\right) = \frac{k_B T_P}{h}\exp\left(-\frac{\Delta G^{\neq}}{RT_P}\right) \quad (2)$$

$$\Delta H^{\neq} = E_k - RT_P \quad (3)$$

$$\Delta G^{\neq} = \Delta H^{\neq} - T_P\Delta S^{\neq} \quad (4)$$

where $A = 1$ when using Kissinger correlation to calculate, T_P is the decomposition peak temperature at heating rate 10 °C min^{-1} in degrees Kelvin, h is the Planck constant, k_B is the Boltzmann constant, E_k is the apparent activation energy, and R is the ideal gas constant. Although the difficulty of molecular activation is determined by the activation energy, $\Delta H^{\neq}$, $\Delta S^{\neq}$, $\Delta G^{\neq}$ can also reflect the changes in the activation process from the thermodynamics point of view. The calculated related thermal property data are presented in Table 2.

As show in Table 2, the $\Delta S^{\neq}$ of DP1 and DP2 are very close to that of NQ and HMX. All $\Delta G^{\neq}$ are positive which means their activating reaction are not spontaneous and the E_a or $\Delta H^{\neq}$ is the required heat energy. However, the $\Delta H^{\neq}$ and $\Delta G^{\neq}$ of DP1 and DP2 are higher than NQ and HMX respectively, which indicates that after co-crystallization the molecule of co-crystal need more energy when occurs to activate. Thus it shows that the thermal stability of ultrafine HMX/NQ co-crystal is superior to raw materials.

3.6. Mechanical sensitivity test

The sensitivity results are listed in Table 3. As shown in the table, the impact sensitivity of the co-crystal decreased to 28% from the significantly higher impact sensitivity of 100% for neat HMX and 76% for the physical mixture. It is conjectured that the intermolecular hydrogen bond increases the stability of

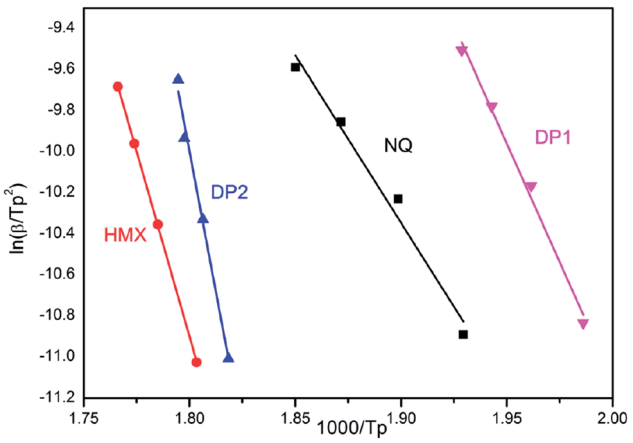

Fig. 8 Dependence of $\ln(\beta/T_P^2)$ on $1/T_P$ for NQ, HMX DP1 and DP2. Scatter points are experimental data and lines denotes the linear fitting results.

Table 2 The related thermal property data of NQ, HMX DP1 and DP2

	E_a/(kJ mol^{-1})	$\Delta H^{\neq}$/ (kJ mol^{-1})	$\Delta S^{\neq}$/ (J mol^{-1} K^{-1})	$\Delta G^{\neq}$/ (kJ mol^{-1})
DP1	192.03	187.79	−257.69	319.16
NQ	135.84	131.46	−257.95	267.32
DP2	456.03	451.43	−258.36	594.46
HMX	299.96	295.30	−258.48	440.10

Table 3 Results of sensitivity test for NQ, HMX, and HMX/NQ co-crystal

Sample	Impact sensitivity P/%
NQ	0
HMX	100
HMX/NQ	28
Physical mixture	76

molecular system of the co-crystal. Moreover, the particle size and spherical morphology are advantageous for reduction of sensitivities.[43,44] Therefore, the effect of reducing the impact sensitivity is obvious.

3.7. Determination of density

Here the density of the ultrafine HMX/NQ co-crystal was tested as 1.80 g cm^{-3} by the drainage method, which is lower than that of HMX (1.94 g cm^{-3}) but much higher than that of NQ (1.58 g cm^{-3}) tested under the same conditions. This can be attributed to the close packing of the co-crystal.

3.8. Storage performance

The storage of the co-crystal was tested by mercury pressure gauge method. The released gas of the co-crystal is 0.002 mL g^{-1} which shares the same level with raw HMX. The result indicates that the product doesn't decompose under the experimental conditions, which shows the good stability and storage performance of the ultrafine co-crystal.

4. Conclusions

Ultrafine HMX/NQ co-crystal was successfully prepared by vacuum freeze drying method. SEM characterized the morphology of co-crystal. The FT-IR, Raman, PXRD further prove the formation of the co-crystal, and to a certain extent, also the existence of intermolecular hydrogen bonds which are the main driving forces. D_{sc} indicated that the thermal stability of the co-crystal explosive was better than the raw materials. The sensitivity result indicated that the mechanical sensitivity of HMX/NQ co-crystal was a little higher than NQ but much lower than HMX. The density of the product was tested as 1.80 g cm^{-3} and the storage performance was as good as HMX. Further application of the ultrafine co-crystal in the area of PBX and propellants will be our future work.

Conflicts of interest

There are no conflicts to declare.

Acknowledgements

This work was financially supported by the Natural Science Foundation of China (Project No. 50972060 and No. 51606102), the Weapon Research Support Fund (62201070804), Qing Lan Project, Environmental Protection Scientific Research Project of Jiangsu Province (2016056), a Project funded by the Priority Academic Program Development of Jiangsu Higher Education Institutions, the Shanghai Aerospace Science and Technology Innovation Fund (SAST2015020), Basic Product Innovation Technology Research Project of Explosives.

Notes and references

1 R. M. Doherty and D. S. Watt, *Propellants, Explos., Pyrotech.*, 2008, **33**, 4–13.
2 L. Borne, J. Mory and F. Schlesser, *Propellants, Explos., Pyrotech.*, 2008, **33**, 37–43.
3 H. Czerski and W. G. Proud, *J. Appl. Phys.*, 2007, **102**, 1–8.
4 N. Radacsi, A. I. Stankiewicz, Y. L. M. Creyghton, A. E. D. M. van der Heijden and J. H. ter Horst, *Chem. Eng. Technol.*, 2011, **34**, 624–630.
5 K. Cowey, S. Day and R. Fryer, *Propellants, Explos., Pyrotech.*, 1985, **10**, 61–64.
6 N. Radacsi, R. H. B. Bouma, E. L. M. K. Haye, J. H. ter Horst, A. I. Stankiewicz and A. E. D. M. van der Heijden, *Propellants, Explos., Pyrotech.*, 2013, **38**, 761–769.
7 E. A. Zhurova, V. V. Zhurov and A. A. Pinkerton, *J. Am. Chem. Soc.*, 2007, **129**, 13887–13893.
8 R. W. Millar, S. P. Philbin, R. P. Claridge and J. Hamid, *Propellants, Explos., Pyrotech.*, 2004, **29**, 81–92.
9 X. Song, Y. Wang, C. An, X. Guo and F. Li, *J. Hazard. Mater.*, 2008, **159**, 222–229.
10 D. E. Chavez, B. C. Tappan, M. A. Hiskey, S. F. Son, H. Harry, D. Montoya and S. Hagelberg, *Propellants, Explos., Pyrotech.*, 2005, **30**, 412–417.
11 R. R. Sanghavi, A. G. S. Pillai, S. P. Velapure and A. Singh, *J. Energ. Mater.*, 2010, **21**, 87.
12 R. S. Damse and A. K. Sikder, *J. Hazard. Mater.*, 2007, **154**, 888–892.
13 D. Braga, F. Grepioni and L. Maini, *Chem. Commun.*, 2010, **46**, 6232–6242.
14 F. Lara-Ochoa and G. Espinosa-Perez, *Supramol. Chem.*, 2007, **19**, 553–557.
15 N. Shan and M. J. Zaworotko, *Drug Discovery Today*, 2008, **13**, 440–446.
16 Ö. Almarsson and M. J. Zaworotko, *Chem. Commun.*, 2004, **17**, 1889–1896.
17 A. V. Trask, W. D. S. Motherwell and W. Jones, *Cryst. Growth Des.*, 2005, **5**, 1013–1021.
18 W. Jones, W. D. S. Motherwell and A. V. Trask, *MRS Bull.*, 2006, **31**, 875–879.
19 D. J. Good and N. RodríGuez-Hornedo, *Cryst. Growth Des.*, 2009, **9**, 2252–2264.
20 N. Qiao, M. Z. Li, W. Schlindwein, N. Malek, A. Davies and G. Trappitt, *Int. J. Pharm.*, 2011, **419**, 1–11.
21 S. G. Fleischman, S. S. Kuduva, J. A. McMahon, B. Moulton, R. D. B. Walsh, N. Rodríguez-Hornedo and M. J. Zaworotko, *Cryst. Growth Des.*, 2003, **3**, 909–919.
22 N. Schultheiss and A. Newman, *Cryst. Growth Des.*, 2009, **9**, 2950–2967.
23 A. N. Sokolov, T. Friščić and L. R. MacGillivray, *J. Am. Chem. Soc.*, 2006, **128**, 2806–2807.
24 C. Y. Guo, H. B. Zhang, X. C. Wang, J. J. Xu, Y. Liu, X. F. Liu, H. Huang and J. Sun, *J. Mol. Struct.*, 2013, **1048**, 267–273.
25 H. Zhang, C. Guo, X. Wang, J. Xu, X. He, Y. Liu, X. Liu, H. Huang and J. Sun, *Cryst. Growth Des.*, 2013, **13**, 679–687.
26 H. Lin, S.-G. Zhu, L. Zhang, X.-H. Peng and H.-Z. Li, *J. Energ. Mater.*, 2013, **31**, 261–272.
27 O. Bolton and A. J. Matzger, *Angew. Chem., Int. Ed.*, 2011, **50**, 8960–8963.
28 J. P. Shen, X. H. Duan, Q. P. Luo, Y. Zhou, Q. L. Bao, Y. J. Ma and C. H. Pei, *Cryst. Growth Des.*, 2011, **11**, 1759–1765.

29 K. Liu, G. Zhang, J. Y. Luan, Z. Q. Chen, P. F. Su and Y. J. Shu, *J. Mol. Struct.*, 2016, **1110**, 91–96.
30 Z. W. Yang, H. Z. Li, X. Q. Zhou, C. Y. Zhang, H. Huang, J. S. Li and F. D. Nie, *Cryst. Growth Des.*, 2012, **12**, 5155–5158.
31 O. Bolton, L. R. Simke, P. F. Pagoria and A. J. Matzger, *Cryst. Growth Des.*, 2012, **12**, 4311–4314.
32 H. F. Xu, X. H. Duan, H. Z. Li and C. H. Pei, *RSC Adv.*, 2015, **5**, 95764–95770.
33 Q. Lv and Q. L. Feng, *J. Mater. Sci.: Mater. Med.*, 2006, **17**, 1349–1356.
34 X. Wu, Y. Liu, X. Li, P. Wen, Y. Zhang, Y. Long, X. Wang, Y. Guo, F. Xing and J. Gao, *Acta Biomater.*, 2010, **6**, 1167–1177.
35 J. Liu, W. Jiang, F. S. Li, L. X. Wang, J. B. Zeng, Q. Li, Y. Wang and Q. Yang, *Propellants, Explos., Pyrotech.*, 2014, **39**, 30–39.
36 J. Y. Wang, H. Q. Li, C. W. An and W. J. Guo, *Chin. J. Energ. Mater.*, 2015, **23**, 1103–1106.
37 H. W. Qiu, R. B. Patel, R. S. Damavarapu and V. Stepanov, *CrystEngComm*, 2015, **17**, 4080–4083.
38 National Military Standard of China, *Experimental Methods of Sensitivity and Safety*, GJB/772A-97, 1997, in Chinese.
39 X. L. Song, Y. Wang, C. W. An, X. D. Guo and F. S. Li, *J. Hazard. Mater.*, 2008, **159**, 222–229.
40 X. L. Song and F. S. Li, *Def. Sci. J.*, 2009, **59**, 37–42.
41 Z. W. Yang, H. Z. Li, H. Huang, X. Q. Zhou, J. S. Li and F. D. Nie, *Propellants, Explos., Pyrotech.*, 2013, **38**, 495–501.
42 T. Chen, W. Jiang, P. Du, J. Liu, G. Z. Hao, H. Gao, L. Xiao and X. Ke, *RSC Adv.*, 2017, **7**, 5957–5965.
43 J. Y. Wang, J. L. Li, C. W. An, C. H. Hou, W. Z. Xu and X. D. Li, *Propellants, Explos., Pyrotech.*, 2012, **37**, 670–675.
44 Y. Bayat, M. Zarandi, M. A. Zarei, R. Soleyman and V. Zeynali, *J. Mol. Liq.*, 2014, **193**, 83–86.